Journal of Materials Chemistry B

Accepted Manuscript

ROYAL SOCIETY OF CHEMISTRY

www.rsc.org/materialsB

Journal Name

RSCPublishing

ARTICLE

pH-Responsive Cancer-targeted Selenium Nanoparticles: A Transformable Drug Carrier with Enhanced Theranostic Effects

Cite this: DOI: 10.1039/x0xx00000x

Received 00th January 2012,
Accepted 00th January 2012

DOI: 10.1039/x0xx00000x

www.rsc.org/

Bo Yu,[a] Xiaoling Li,[a] Wenjie Zheng,*[a] Yanxian Feng,[a] Yum-Shing Wong[b] and Tianfeng Chen*[a]

Selenium nanoparticles (SeNPs) have been widely used in various biomedical applications, including cancer therapy, diagnosis and drug delivery. Herein, we fabricated a novel type of structure-transformable capsules by decoration of SeNPs with folate-chitosan to form smart-shell nanocapsules (FAC@CurP-SeNPs). The shrink particles could target cancer cells over expressing folate receptor and enter the cells via folate receptor-mediated endocytosis. FAC@CurP-SeNPs were expanded to snowflake particles under acidifying stimulus (pH 5.3), which led to enhanced drug-release over prolonged periods. Treatment with FAC@CurP-SeNPs significantly inhibited the growth of MCF-7 human breast carcinoma cells through induction of apoptosis, which was evidenced by accumulation of sub-G1 cell population, DNA fragmentation and nuclear condensation. The contribution of extrinsic and intrinsic apoptotic pathways to the cell apoptosis was confirmed by activation of caspase-9 and caspase-8. Internalized FAC@CurP-SeNPs triggers intracellular ROS overproduction, thus activates p53, MAPKs pathways and inhibits NFκB and to promote cell apoptosis. Our results suggest that FAC@CurP-SeNPs may be a candidate for further evaluation as a agent for human cancers, and the strategy to use transformable nanocapsules could be a highly efficient way to enhance controlled drug release and anticancer efficacy.

1 Introduction

Nowadays, one of the most critical obstacles for cancer chemotherapy is the limited availability of effective delivery systems for hydrophobic anticancer drugs, since low drug solubility in aqueous media prevents their intravenous administration. However, over 40% of small-molecule anticancer drugs produced by pharmaceutical companies have poor water solubility [1]. Therefore, it is of great significance to construct nanodrug delivery systems for anticancer drugs to enhance their solubility and action efficacy. The combination of biotechnology and nanotechnology has led to the development of cancer nanotechnology that displays application potential in targeted therapy, molecular diagnosis and molecular imaging [2-5]. Nanodrug delivery systems are expected to depress the toxic side effects and simultaneously enhance the therapeutic efficiency [6]. Various sophisticated techniques have been developed to create physical structures that could be used for efficient encapsulation of active ingredients, such as vitamins, proteins, genes and chemical drugs [7]. Precise control of the size, mechanical strength, and compatibility of the encapsulation structures would allow the strategic design of possible release mechanisms [8]. Recently, various encapsulation structures have been investigated widely, including lipid vesicles and polymer capsules, and hollow spheres composed of hybrids and inorganic materials including silica, carbon, quantum dots, selenium and metal[9-11]. Some practical applications often require robustness and flexibility in encapsulation materials [12]. Obviously, these properties are frequently mutually exclusive. For instance, highly robust inorganic materials lack the advantageous flexibility of soft organic ones. Thus, the manipulation of encapsulation inorganic materials were still one of the most important and challenging tasks in this field.

Researchers have extensively explored nanosized encapsulation systems that could be easily extravasated from the tumor's leaky blood capillaries and preferentially deliver the loaded drugs to cancer tissues by enhanced permeability and retention effect during cancer chemotherapy [13]. Stimuli-sensitive drug delivery is a promising strategy for achieving on-demand release of drugs [14]. External and internal stimuli, including temperature [15], pH [16, 17], ultrasound [18], light [19], chemical reactions [20] and protease [21] could be utilized to regulate the release of drugs in various delivery systems [22].

Among those strategies, targeted-release based on pH variation has received the greatest attention. In the case of cancer therapy, the pH difference between normal and cancer cells could be used for targeting drug design. The pH values in the human body naturally varies between the different organs and tissues, which make the pH-triggered approach one of the most efficient strategies for drug delivery [23]. Furthermore, encapsulation decorated with targeting groups such as folic acid (FA), and Arginine-Glycine-Aspartic acid (RGD) can specifically target and be efficiently uptake by cancer cells that overexpress their receptors by endocytosis, and deliver drugs into the cytosol [24, 25]. Till now, various interesting nano or micron encapsulation, such as silica microcapsules with changed size shell [26], silica nanocases with hollow shell [27], gold nanorattles [28] and platinum open-mounthed microcapsules [9], have been developed. However, the above-mentioned encapsulation structure only supplied the inorganic surface without providing ample outer layers that could be decorated and functionalized by targeted ligands. Selenium nanoparticles (SeNPs) have attracted more and more attention in the past decade, due to their high bioavailability, low toxicity and novel therapeutic properties by comparing with other selenium species [29-32]. Recently, we have reported the strategy to use SeNPs as a carrier of hydrophobic anticancer drugs to achieve anticancer synergism [33]. This strategy brings new horizon for cancer therapy and opens a new area for application of SeNPs. And our recently work described the synthesis of DOX-loaded and Tf-conjugated SeNPs (Tf-SeNPs) and its use as a cancer-targeted drug delivery system to achieve enhanced cellular uptake and anticancer efficacy[34]. However, limitation still exists in this drug delivery system. The unstability of Tf will affect the lifetime and circulation of the nanosystem in our human bodies. Moreover, the fast drug release rate may also limit its future application. Therefore, improvement is needed for using SeNPs as drug carriers.

Curcumin, a low-molecular-weight natural fluorescence polyphenolic compound, has been found to have a wide range of biological and pharmacological activities, such as antioxidant, anti-inflammatory and anticancer properties [35]. Curcumin inhibited the expression of several cellular targets in cancer cells like NF-κB and AKT, and thus induced cell apoptosis [36]. Curcumin was also proved to be a safe agent for *in vivo* application, since no signs of toxicity were found in animals or humans treated with Curcumin [37]. Unfortunately, the further clinical application of Curcumin also was limited by its poor solubility in aqueous solution, poor oral bioavailability. Therefore, an aqueous formulation with controlled release property is desired for clinical application of curcumin. Herein, we present a cancer-targeted drug delivery system that allows the direct fluorescence monitoring of the cellular uptake and localization of theranostic agents in cancer cells, by the combination of robust inorganic SeNPs with the high diversity surface flexibility materials-chitosan (CS) and using FAC as a targeting ligand. Compared with our previous Tf-SeNPs, this nanosystem combinated two nutrient elements, curcumin and selenium, as targeted drugs. It exhibits three folds anticaner activities to MCF-7 cells and characteristic of shape transformation and pH-controlled drug release that allow the facilitated release of entrapped CurP within acidifying intracellular compartments such as endosomes and lysosomes.

2 Materials and methods

Materials.

Selenium dioxide, polyvinyl pyrrolidone (PVP, average MW 40000), folic acid (FA), curcumin (Cur), 4-dimethylaminopyridine (DMAP), 1-(3-Dimethylaminopropyl)-3-ethylcarbodiimide hydrochloride (EDC), triethyl amine (TEA), 3-(4,5-dimethylthiazol-2-yl)-2,5 diphenyltetrazolium bromide (MTT), pro-pidium iodide (PI), and ascorbic acid (AA) were purchased from Sigma-Aldrich Chemical Co. Annexin-V-FLUOS staining kit and in situ cell death detection kits were obtained from Roche Molecular Biochemicals. The water used for all experiments was ultrapure, supplied by a Milli-Q water purification system from Millipore. All of the solvents used were of HPLC grade. Chitosan, with a molecular weight of 60000 g/mol and the degree of deacetylation was 90.0%, was purchased form Beijing Ribio Biotech Co., LTD. Dimethyl sulfoxide (DMSO) was purchased from Guangzhou Chemical Reagent Factory.

Synthesis of curcumin-polyvinyl pyrrolidone conjugate (CurP).

The conjugate was synthesized as reported earlier with a minor change[38]. About 3 g of PVP, 1 g DMAP, 2 mL TEA and 200 mg of curcumin were added in to 100ml of DMSO in a 250 mL RB flask with N_2 protection. The reaction mixture was stirred well at 45 ℃ for about 12 h. The resultant solution was dialyzed against DMSO for 3 days and then against deionized water for 7 days using a dialysis membrane (MWCO: 8000 Da) to remove unbound entities. CurP was lyophilized and kept under refrigeration.

Synthesis of folic acid-chitosan conjugate (FAC).

The conjugate was synthesized as reported earlier with a minor change[39]. A solution of folic acid and EDC in 20 mL DMSO (molar ratio was 1:1) was prepared and stirred at RT until EDC and folic acid were well-dissolved and mixed. The mixture was then added to 1% (w/v) chitosan in acetic acid aqueous solution and stirred at RT in the dark for 24 h to let folic acid conjugate onto chitosan molecules (molar ratio was 2:1). The solution was brought to pH 9.0 by dripping with NaOH aqueous solution (1.0 M) and centrifuged at 2500 rpm to spin down the folic acid–chitosan conjugate (FAC). The precipitate was dialyzed against water for 7 days. Finally, the FAC was isolated as a sponge by lyophilization and kept for follow-up study.

Preparation of CurP-SeNPs.

The process of conjugation of CurP to selenium nanoparticles (SeNPs) is described as follows with minor change[40]: The solution of 100 mM ascorbic acid was freshly prepared. As a

typical procedure, CurP solution was dropwise added into 1 ml of 125 M H_2SeO_3 solution under magnetic stirring, and then 5 mL of 100 mM ascorbic acid solution was added into the mixture and then it was reconstituted to a final volume of 25 mL with Milli-Q water. The final concentration of Se was 5 mM, and the reactant concentration of CurP was 1 mg/mL. The solution was dialyzed against Milli-Q water until no Se was detected in the outer solution by ICP-AES analysis. Finally, the CurP-SeNPs were isolated by concentration and lyophilization and kept for follow-up study.

Preparation of FAC@CurP-SeNPs.

The preparation process is briefly described as follows: 0.5% FAC solutions were prepared by dissolving FAC in 5 mL acetic acid solution at pH 5.3. CurP-SeNPs solution was prepared by ultrasonic dispersing CurP-SeNPs powder in Milli-Q water with 37 kHz 15 min. Then, CurP-SeNPs solution was dropwise added into FAC solution under magnetic stirring for 12 h, and it was reconstituted to a final volume of 25 mL with acetic acid solution. The final concentration of Se was 5 mM, and the reactant concentration of FAC was 0.5 mg/mL. The solution was dialyzed against PBS solution (pH 7.4) until no Se was detected in the outer solution by ICP-AES analysis. Finally, the FAC@CurP-SeNPs was isolated by concentration and lyophilization and kept for follow-up study. The loading content of curcumin[41] and folic acid[39] in the nanoparticles were analyzed as previously described by spectrophotometry (Versamax).

Characterization of materials.

The shapes and crystalline structures of as-prepared products were characterized by using microscopic and spectroscopic methods. Briefly, TEM samples were prepared by dispersing the powder particles onto holey carbon film on copper grids. The micrographs were obtained on Hitachi (H-7650) for TEM operated at an accelerating voltage at 80 kV. And the Philips TECNAI 20 high-resolution transmission electron microscopy (HRTEM) worked at 400 kV. TEM-EDX analysis was carried out on the Philips TECNAI 20 high-resolution transmission electron microscopy and employed to examine the elemental composition of FAC@CurP-SeNPs. The size distribution of the nanoparticles was measured by PCS on a Nano-ZS instrument (Malvern Instruments Limited). Fourier transform infrared spectroscopy (FT-IR) spectra of the samples were recorded on Equinox 55 IR spectrometer in the range 4000-400 cm^{-1} using the KBr-disk method.

Determination of Se.

Se concentration was determined by ICP-AES method[42]. The digested product was reconstituted to 10 ml with Milli-Q H_2O and used for ICP-AES analysis.

Cell lines and cell culture.

Several human cancer cell lines, including A375 melanoma cells, HepG2 hepatocellular carcinoma cells, MCF-7 breast adenocarcinoma cells and A549, were purchased from American Type Culture Collection (ATCC, Manassas, VA). All cell lines were maintained in either RPMI-1640 or DMEM media supplemented with fetal bovine serum (10%), penicillin (100 units/ml) and strep-tomycin (50 units/ml) at 37 ℃ in CO_2 incubator (95% relative humidity, 5% CO_2).

MTT assay.

Cell viability was determined by measuring the ability of cells to transform MTT to a purple formazan dye[43]. The cells were then incubated with FAC@CurP-SeNPs at different concentrations for different periods of time.

Flow cytometric analysis.

The cell cycle distribution was analyzed by flow cytometry as previously described[44]. Apoptotic cells with hypodiploid DNA content were measured by quantifying the sub-G1 peak in the cell cycle pattern. For each experiment, 10,000 events per sample were recorded.

TUNEL-DAPI co-staining assay.

DNA fragmentation induced by FAC@CurP-SeNPs was examined by using an in situ cell death detection kit following the manufacturer's protocol[45].

Intracellular localization of FAC@CurP-SeNPs.

The intracellular localization of FAC@CurP-SeNPs in MCF-7 cells was traced with the lysosomal marker Lyso Tracker Red staining. Briefly, the cells cultured on cover glass in 6-well plates till 70% confluence were stained with 80 nM lyso-tracker DND-99 (Molecular Probes) and 1 μg/mL DAPI for 2 h and 20 min, respectively. After washing with PBS twice, the cells were incubated with FAC@CurP-SeNPs for various periods of time and examined under the Zeiss LSM 510 Meta laser scanning confocal microscope systems.

***In vitro* drug release of FAC@CurP-SeNPs.**

Two copies of 10 mg of FAC@CurP-SeNPs were respectively suspended in 10 ml PBS solution at pH 5.3 and pH 7.4 with constantly shaking in dark tubes at 37°C. At specific intervals, a certain volume of buffer was taken out from tubes and same volume of fresh buffer was replaced. The collected buffer was centrifuged and the CurP concentration was detected by modification of a literature method with fluorescence microplate reader[46]. (With excitation and emission wavelength set as 430 nm and 530 nm respectively).

Caspase activity.

The cell lysates and specific caspase substrates (Ac-DEVD-AMC for caspase-3, Ac-IETD-AMC for caspase-8, and Ac-LEHD-AMC for caspase-9) were added into 96-well plates at

37°C for 2 h. Caspase activity was measured by fluorescence intensity with the excitation and emission wavelength set as 380 nm and 460 nm respectively.

Western blot analysis.

The effects of FAC-SeNPs on the expression levels of proteins associated with different signaling pathways were examined by Western blot analysis[47]. MCF-7 cells treated with FAC@CurP-SeNPs (2 μM, IC_{50} value), FAC-SeNPs (10 μM, IC_{50} value), CurP (140 μg/mL, IC_{50} value), respectively for 24 h were incubated with lysis buffer (Beyotime) to obtain total cellular proteins. The protein concentration was examined by BCA assay.

Statistical Analysis.

All experiments were carried out at least in triplicate and results were expressed as mean ± S.D. Statistical analysis was performed using SPSS statistical program version 13 (SPSS Inc., Chicago, IL). Difference between two groups was analyzed by two-tailed Student's t-test. Difference with $P < 0.05$(*) was considered statistically significant. The difference between three or more groups was analyzed by was analyzed by one-way ANOVA multiple comparisons.

3 Results and discussion

Preparation and characterization of FAC@CurP-SeNPs.

This transformable nanosystem was fabricaeted by combination of CurP-SeNPs carrier with FAC to form smart-shell nanocapsules. The results of TEM characterization revealed the conversion of the starting material (rough-surfaced and small particles at about 200 nm, Fig. 1A) to snowflake objects with larger diameters at about 500 nm (Fig. 1B), while the pH value of FAC@CurP-SeNPs dispersed solution changed from 7.4 to 5.3. The size of small nanoparticles on the snowflake objects was about 10~20 nm (Fig. 1B), which was the same as those showed in Fig. S2a. The products were further characterized by TEM-EDX and high-resolution transmission electron microscopy (HRTEM). The results of HRTEM (Fig. 1C) showed that the lattice pattern (left) and corresponding SAED pattern (right) of the FAC@CurP-SeNPs obtained at RT, which revealed that the lattice fringe was 0.329 nm. The elemental composition analysis (TEM-EDX) showed the presence of strong signals from the Se atoms, together with C atom signal from FAC and CurP (Fig. 1D). As shown in Fig. 1E and Fig. S2b, the particles size of SeNPs without capping agent were about 1 μm, while CurP-SeNPs were about 10~20 nm. The size of resulting material, FAC@CurP-SeNPs, was about 200 nm in PBS solution, and changed to 500 nm after dispersed in PBS solution (5.3) for 6 h. Finally, the size enlarged to several hundreds of nanometers after 24 h acid treatment (Fig. S3). The significance of zeta potential can be related to the stability of colloidal dispersion. In this paper, the corresponding zeta

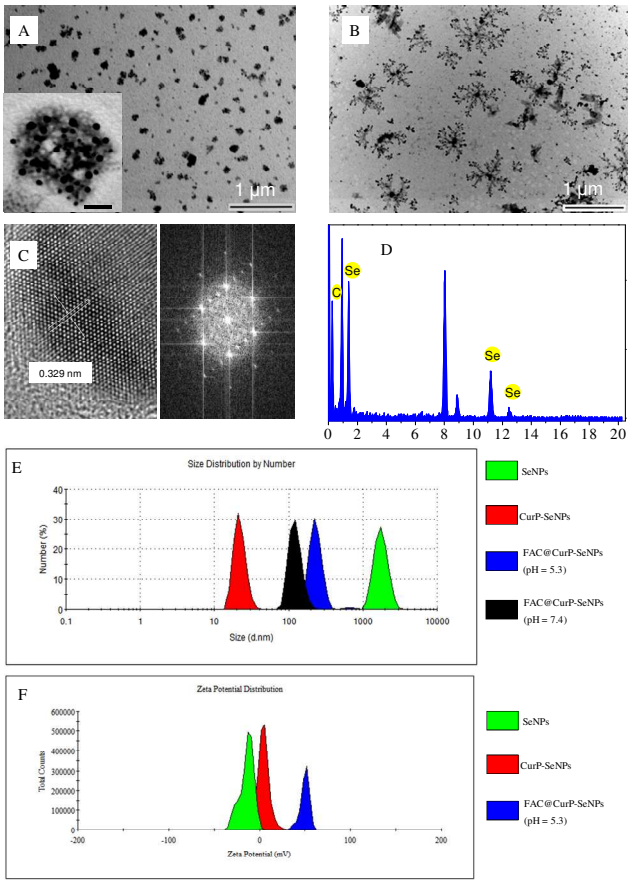

Fig. 1. Structural characterization of FAC@CurP-SeNPs. (A) Representative TEM images of FAC@CurP-SeNPs diffused in PBS (pH 7.4, inset show enlarge images, scale bar is 100 nm) or (B) acid PBS solution (pH 5.3), lattice fringes and corresponding SAED pattern (C), EDX analysis of FAC@CurP-SeNPs (D), and (E) Representative size distribution, (F) Zeta potential of SeNPs, CurP-SeNPs and FAC@CurP-SeNPs diffused in PBS solution (pH 7.4, pH 5.3).

potential shown that the value of zeta potential of SeNPs, CurP-SeNPs, FAC@CurP-SeNPs were -18, -1 and +50 mV (Fig. 1F),respectively. These results suggest the reaction of CurP-SeNPs and FAC, and coincide with the TEM results that CurP-SeNPs were capped by FAC. The loading content of curcumin and folic acid in the nanoparticles were found at 0.31% and 1.54%, respectively.

Induction of cancer cell apoptosis by FAC@CurP-SeNPs.

Folate Receptor (FR) is overexpressed in many human cancer cells, including ovary, brain, kidney, breast, myeloid and lung cancers. FR constitutes as a useful targeting site for tumor-specific drug delivery. In this study, the *in vitro* cytotoxic by MTT assay of FAC@CurP-SeNPs were first screened against MCF-7 (folic acid recptor positive), A549 and A375 cells (folic acid recptor negative). As shown in Fig. 2A, FAC@CurP-SeNPs exhibited a broad-spectrum inhibition against MCF-7, A549, A375 cells with IC_{50} values ranging from 2.4 to 35.9 μM. Under the corresponding conditions, the IC_{50} values for

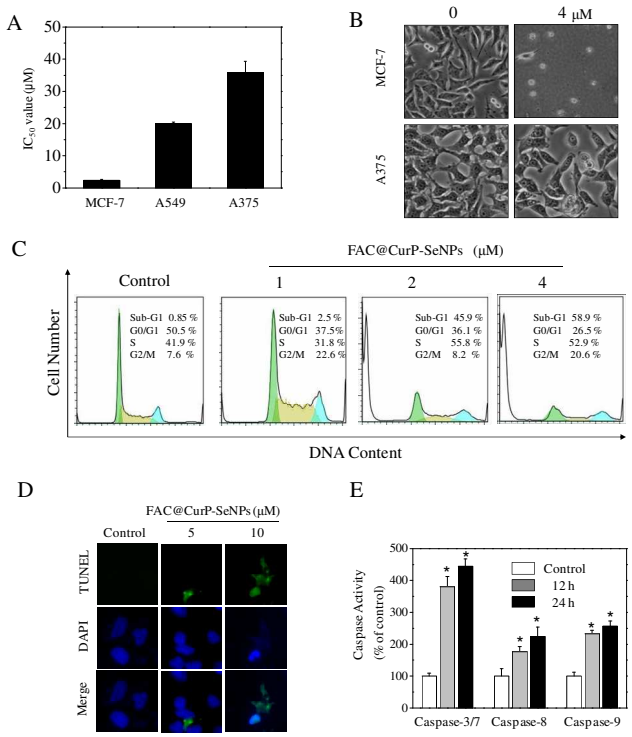

Fig. 2. *In vitro* anticancer activities of FAC@CurP-SeNPs. A) Growth inhibition of FAC@CurP-SeNPs on selected human cancer cell lines (72 h). B) Morphology of MCF-7 and A375 cells treated with FAC@CurP-SeNPs for 72 h (magnification, 200×). C) Flow cytometric analysis of apoptosis and change in cell cycle distribution of MCF-7 cells treated with FAC@CurP-SeNPs for 72 h. D) DNA fragmentation and nuclear condensation induced by FAC@CurP-SeNPs in MCF-7 cells by TUNEL-DAPI co-staining assay. Cells were treated with FAC@CurP-SeNPs for 24 h. Magnification, 400 ×. E) FAC@CurP-SeNPs induced caspase activation. MCF-7 Cells were treated with FAC@CurP-SeNPs for 12 and 24 h. Significant difference between treatment and control groups is indicated at $P < 0.05$ (*) level.

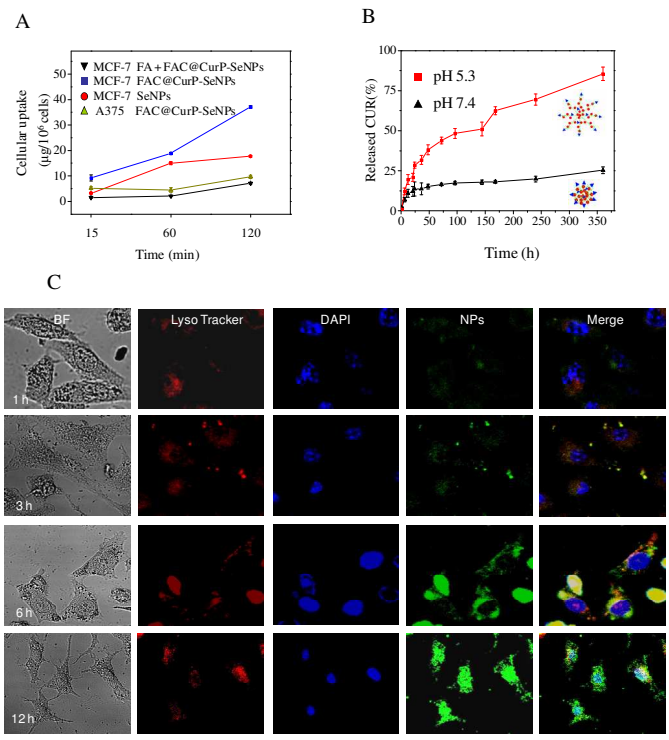

Fig. 3. Selective cellular uptake, drug release and intracellular localization of FAC@CurP-SeNPs. A) Quantitative analysis of cellular uptake efficiency of FAC@CurP-SeNPs by A375 and MCF-7 cells, B) In vitro release profiles of CurP from FAC@CurP-SeNPs in PBS solution at pH 7.4 (black), in acetic acid solution at pH 5.3 (red). C) Intracellular fate of FAC@CurP-SeNPs. MCF-7 cells labeled with DAPI (nucleus) and Lyso Tracker Red (lysosome) were treated and FAC@CurP-SeNPs at 37 ℃ for different periods of time and visualized under Confocal microscope. Values expressed are mean ± SD of triplicates.

FAC, CurP, SeNPs, FAC-SeNPs, CurP-SeNPs and FAC@CurP-SeNPs on MCF-7 cells were found at 188.8 μg/mL, 146.1 μg/mL, 178.5 μM (14.3 μg/mL), 10.3 μM (0.824 μg/mL), 11.7 μM (0.944 μg/mL) and 2.4 μM (0.912 μg/mL), respectively (Fig. S4A). Moreover, the isobologram analysis showed that, the location of the data point in the isobologram was far below the line defining an additive effect. Moreover, the CI value for FAC@CurP-SeNPs was found at 0.056. These results suggest that the growth inhibitory effect between CurP and SeNPs was strongly synergistic (Fig. S4B). Moreover, the results of phase-contrast observation (Fig. 2B) show that MCF-7 cells treated with FAC@CurP-SeNPs for 72 h exhibited dose-dependent reduction in cell numbers, loss of cell-to-cell contact, cell shrinkage and formation of apoptotic bodies, which suggest the induction of apoptotic cell death. The inhibition on cancer cell proliferation by anticancer drugs could be the results of induction of apoptosis or cell cycle arrest, or a combination of these two modes. Therefore, we performed PI-flow cytometric analysis to determine what mechanisms were involved in the cell death induced by FAC@CurP-SeNPs. The results reveal that exposure of MCF-7 cells to different concentrations of FAC@CurP-SeNPs led to dose-dependent increase in the proportion of apoptotic cells, as reflected increase by the Sub-G1 populations (Fig. 2C). For instance, treatment of MCF-7 cells with 4 μM FAC@CurP-SeNPs resulted in the Sub-G1 peak from 0.85% (control) to 58.9%. In contrast, no significant changes in cell cycle distribution of G0/G1, S and G2/M phases were observed in treated cells. Moreover, the results of phase-contrast observation (Fig. S5) show that MCF-7 cells treated with FAC@CurP-SeNPs exhibited dose-dependent reduction in cell numbers, loss of cell-to-cell contact, cell shrinkage and formation of apoptotic bodies, which suggest the induction of apoptotic cell death. Apoptotic cell death was further confirmed by DNA fragmentation and nuclear condensation as examined by TUNEL and DAPI co-staining assay. DNA fragmentation has been regarded as an important biochemical hallmark of cell apoptosis. TUNEL staining is an effective way to detect early stage of DNA fragmentation in apoptotic cells prior to changes in morphology. As shown in Fig. 2D, after exposure of the cells to FAC@CurP-SeNPs for 24 h, MCF-7 cells exhibited dose-dependent increase in DNA fragmentation, nuclear condensation and formation of apoptotic bodies. Caspases, a family of cysteine proteases, plays important roles in the initiation and execution of apoptosis. To determine whether caspase activation is involved in the FAC@CurP-SeNPs-induced cell death, the activities of initiator caspases (caspase-8

and caspase-9) and effecter caspases-3/7 were examined by fluorometric assays. Fig. 2E show FAC@CurP-SeNPs evoked activation of caspase-3/7, caspase-8, and caspase-9 in the MCF-7 cells in a time-dependent manner, which suggests that both intrinsic and extrinsic apoptotic pathways were involved in the FAC@CurP-SeNPs-induced apoptosis. Taken together, these results demonstrate that the major mode of cell death induced by FAC@CurP-SeNPs is cell apoptosis.

Selective cellular uptake, intracellular localization and release of FAC@CurP-SeNPs.

Selective cellular uptake of therapeutic drugs remains a formidable obstacle for cancer therapy. Specific ligand-mediated targeting may be a feasible strategy to solve this problem. Herein, A375 and MCF-7 cells were incubated with FAC@CurP-SeNPs for 15, 60, 120 min, respectively. As shown in Fig. 3A, the intracellular FAC@CurP-SeNPs concentrations increased in a time dependent manner. In MCF-7 cells, after 15, 60 and 120 min incubation with FAC@CurP-SeNPs, the intracellular concentration increased to 9.2, 18.9, 37.1 μg per 10^6 cells, respectively, which were about 5-9 times high than that of A375 cells. To confirm the role of folate in the cell uptake, we also examined the cellular uptake of CurP-SeNPs and FAC@CurP-SeNPs blocked with or without FAC in MCF-7 cells treated in the same conditions. Compared the uptake result of FAC@CurP-SeNPs with CurP-SeNPs, we found that the intracellular concentration of FAC@CurP-SeNPs were about 1.2-2.9 times high than that of CurP-SeNPs without FAC capped. Interestingly, after pre-incubated with 100 μg/mL FAC, the uptake amount of FAC@CurP-SeNPs decreased obviously to 5.2, 4.5, 9.7 μg/mL per 10^6 cells after 15, 60, 120 min, respectively. Those results definitely revealed that FAC surface decoration efficiently enhanced the cellular uptake of CurP-SeNPs, and the FAC capped system could be a potential carrier for drugs. Structural flexibility of snowflake objects should facilitate control of release of molecules in drug-carrier applications. The *in vitro* drug release of CurP from FAC@CurP-SeNPs in PBS solution at pH 7.4 (Fig. 3B) and in acetic acid solution at pH 5.3 (Fig. 3B (red)) was investigated to simulate the normal body blood and acidic environments. The cumulative release result of CurP shown pH treatment of the FAC@CurP-SeNPs affected the release behavior. The mainly different occurred after 48 h under two pH systems, which reached 38.1% at pH 5.3 and 15.2% at pH 7.4 within 48 h, respectively. Thereafter, the cumulative release of CurP reached 85.5% at pH 5.3 and 25.3% at pH 7.4 for 360 h, respectively. The results also demonstrated that the release process at pH 7.4 was much slower than that at pH 5.3. This initial similar release amount of CurP, under two different pH solutions, could be partly attributed to the strong capped of CurP-SeNPs in FAC@CurP-SeNPs and slowly shape change from shrinkage particles to snowflake object at pH 5.3 lead to slowly release of CurP from CurP-SeNPs. Moreover, because the shape of FAC@CurP-SeNPs maintained shrinkage particles at pH 7.4 prevent the release of CurP. Therefore, the fast and slow processes might be attributed to release profiles of CurP entrapped in shrinkage FAC@CurP-SeNPs (pH 7.4) or snowflake FAC@CurP-SeNPs (pH 5.3), respectively and prolonged stable drug release system was developed. This sustained release formulations may create a steady drug release profile making the drug substance available over an extended period of time following ingestion, and reduce adverse side effects of free drugs, thus enhance its future application potential.

Endocytosis is one of the most important entry mechanisms that influence the biodistribution for extracellular materials, particularly nanomaterials. In this study, the localization FAC@CurP-SeNPs in MCF-7 cancer cells was investigated by using specific probes, Lyso Tracker Red and DAPI, for fluorescence imaging of lysosomes and cell nucleus, respectively. As shown in Fig. 3C, the combination of the blue, red and green fluorescence clearly indicates the colocalization of FAC@CurP-SeNPs and lysosomes in MCF-7 cells after 1 h and increased in a time-dependent manner. FAC@CurP-SeNPs escaped from lysosomes after 3 h and released into cytosol and distributed in cells after 6 h. During the 6 h to 12 h process, the fluorescence from FAC@CurP-SeNPs changed sharply. These results suggest that the release of CurP was a slow process and FAC@CurP-SeNPs could be an prolonged drug release system.

Activation intracellular apoptotic signaling pathways by FAC@CurP-SeNPs.

Western blotting was employed to confirm apoptosis in MCF-7 cells at the protein level. As shown in Fig. 4A, FAC@CurP-SeNPs induced poly ADP ribose polymerase (PARP) cleavage, a protein serving as a biochemical hallmark of cells undergoing apoptosis and decrease of caspase-7 in a dose-dependent manner, indicating that FAC@CurP-SeNPs activates caspase-mediated apoptosis. As shown in Fig. 4B, expose of MCF-7 cells to the treatment of FAC@CurP-SeNPs resulted in more effectively decrease of caspase-7, which subsequently induced the proteolytic cleavage of PARP. However, CurP or FAC-SeNPs alone showed no obviously effects on caspase-7 and PARP activation.

It is well known that excess production of ROS results in continuous and accumulative oxidative damage to cellular components, alters many cellular signaling pathways during chemotherapy, and leads to apoptotic cell death [48]. In order to investigate whether FAC@CurP-SeNPs trigger ROS-mediated apoptosis, we examined the intracellular ROS level by measuring dicholorofluorescein (DCF) fluorescence intensity. The intracellular ROS generation was measured by using a fluorescent probe DCF. The assay is based on the cellular uptake of a non-fluorescent probe (DCFH-DA), which is subsequently hydrolyzed by intracellular esterases to form dichlorofluorescin (DCFH). This non-fluorescent substrate is oxidized by intracellular ROS producing a fluorescent product DCF. The MCF-7 cells were treated with FAC@CurP-SeNPs, FAC-SeNPs and CurP respectively following incubation with the fluorescent probe DCFH-DA. As shown in Fig. 5A, during the 90 min incubation, only slight increase in intracellular ROS generation was observed in cells exposed to FAC-SeNPs or CurP alone. In contrast, the FAC@CurP-SeNPs treatment induced much higher intracellular ROS generation in MCF-7 cells. MAPKs and PI3K/Akt pathways are major oxidative stress-sensitive signal transduction pathways in most cell types exposed to excess ROS [49, 50]. MAPKs family, including Erk, p38 MAPK and JNK, plays important roles in regulation of cell fate in responses to stress conditions. Among them, Erk could prevent cell apoptosis by blocking the activation of caspase and control the cell differentiation, proliferation and motility [51, 52].

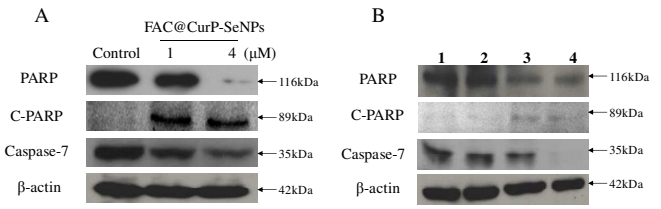

Fig. 4. Induction of apoptosis by FAC@CurP-SeNPs in MCF-7 cells. (A) Effects of FAC@CurP-SeNPs on the expression levels of apoptosis-associated proteins PARP and Caspase-7 was analyzed by western blotting,(B)Western blot analysis the quantitative of PARP cleaved and caspases in the apoptosis induced by SeNPs or/and CurP. Equal protein loading was confirmed by Western analysis of β-actin in the protein extracts (**1** was control, **2** was CurP, **3** was FAC-SeNPs, **4** was FAC@CurP-SeNPs).

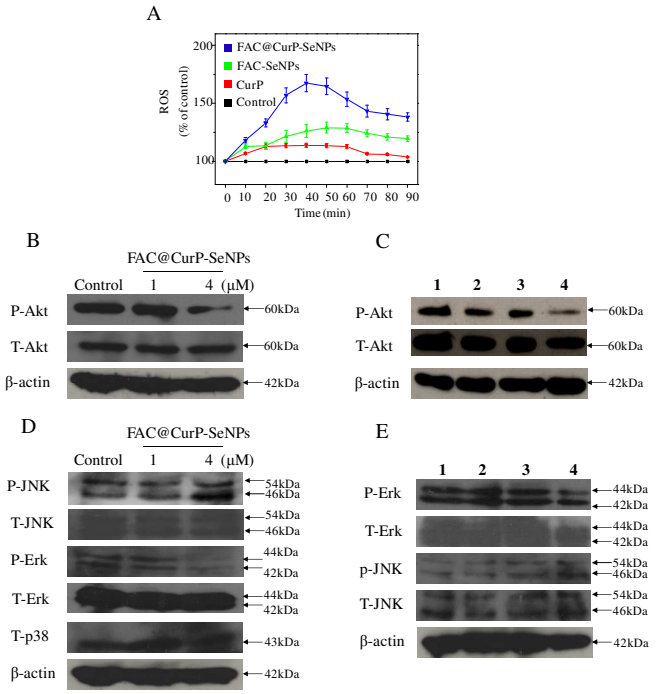

Fig. 5. Effects of FAC@CurP-SeNPs on Akt and MAPKs signaling pathways. (A) Effects of SeNPs or/and CurP on ROS generation in MCF-7 cells. MCF-7 cells were washed and treated with FAC@CurP-SeNPs, SeNPs and CurP after treatment with 10 mM DCFH-DA for 25 min, Fluorescence was analyzed as described in section of Materials and methods. (B) Effects of FAC@CurP-SeNPs on the phosphorylation status and the expression level of Akt,(C)Western blot analysis the quantitative of Akt in the apoptosis induced by SeNPs or/and CurP, (D) Effects of FAC@CurP-SeNPs the phosphorylation and expression level of ERK, p38MAPK and JNK,(E)Western blot analysis the quantitative of ERK and JNK in the apoptosis induced by SeNPs or/and CurP, Equal protein loading was confirmed by detection of β-actin (**1** was Control, **2** was CurP, **3** was FAC-SeNPs, **4** was FAC@CurP-SeNPs).

To determine the possible role of MAPKs in FAC@CurP-SeNPs -induced apoptosis, we checked the status of MAPKs in treated cells. The results of Western blot analysis showed that FAC@CurP-SeNPs in a dose-dependent manner exhibited more significant effect on the expression of phosphorylation Akt than the effect of FAC-SeNPs or CurP alone (Fig. 5B and

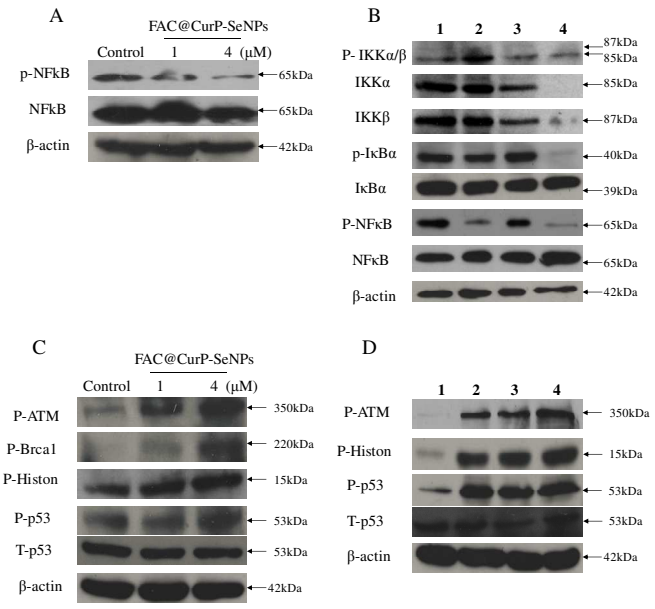

Fig 6. FAC@CurP-SeNPs downregulates NFκB while inhibiting phosphorylates IκBα and DNA damage-mediated p53 activation (A) Effects of FAC@CurP-SeNPs on the expression levels of NFκB was analyzed by western blotting,(B)Western blot analysis the quantitative NF-κB Pathway associated proteins in the apoptosis induced by SeNPs or/and CurP, (C) Effects of FAC@CurP-SeNPs on the expression levels of DNA damage associated proteins was analyzed by western blotting, (D)Western blot analysis the quantitative of p-ATM, p-Histon, and p53 in the apoptosis induced by SeNPs or/and CurP, Equal protein loading was confirmed by Western analysis of β-actin in the protein extracts (**1** was Control, **2** was CurP, **3** was FAC-SeNPs, **4** was FAC@CurP-SeNPs).

C). The results of Western blot analysis revealed that FAC@CurP-SeNPs activated triggered the phosphorylation of JNK and down-regulated phosphorylation Erk (Fig. 5D and E). Taken together,these results suggest that regulation of JNK and Erk pathway contributes to apoptosis induced by FAC@CurP-SeNPs.

The transcriptional nuclear factor κB (NF-κB), a proinflammatory and prosurvival transcription factors, has a central role in inflammation and is known to be constitutively expressed in cancers [53]. NF-κB was present in the cytosol in an inactive state, complexed with the inhibitory IκB proteins[54]. IκB kinase (IKK) phosphorylates IκB at serine residues 32 and 36, triggering its ubiquitination and proteasomal degradation, thereby unmasking the nuclear localization signal of NFκB[55]. In the nucleus, NFκB binds DNA thus enhancing the transcription of various gene products that regulate proliferation, apoptosis, angiogenesis, invasion, inflammation and metastasis. In this study, the results of Western blot analysis showed that FAC@CurP-SeNPs downregulates phosphorylation of NFkB in a dose-dependent manner (Fig. 6A). As shown in Fig. 6B, FAC@CurP-SeNPs exhibited more significant inhibiting effect on the expression of phosphorylation NFκB than FAC-SeNPs or CurP alone. To determine drug effects on IκB, the upstream inhibitor of NFκB, cells were exposed to CurP, FAC-SeNPs and FAC@CurP-

SeNPs and proteins were extracted for immunoblotting against IκBα and p-IκBα. The results of

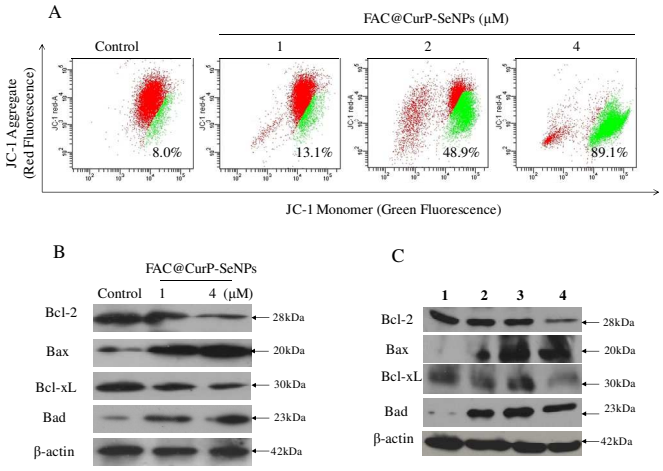

Fig. 7. (A) Depletion of mitochondrial membrane potential in MCF-7 cells induced by FAC@CurP-SeNPs. Cells were treated with FAC@CurP-SeNPs for 24 h, stained with a mitochondria-selective dye JC-1, and analyzed by flow cytometry. The number indicated in each histogram represents the percentage of cells that emit green fluorescence due to the depletion of mitochondrial membrane potential. (B) Western blot analysis of the expression levels of Bad, Bcl-xl, Bax, Bcl-2 in MCF-7 cells, (C)Western blot analysis the quantitative of of Bad, Bcl-xl, Bax, Bcl-2 in the apoptosis induced by SeNPs or/and CurP. Equal protein loading was confirmed by Western analysis of β-actin in the protein extracts (**1** was Control, **2** was CurP, **3** was FAC-SeNPs, **4** was FAC@CurP-SeNPs).

Western blot analysis revealed that FAC@CurP-SeNPs inhibited triggered the phosphorylation of IκBα and down-regulated phosphorylation IKKα/β, suggesting that the observed inhibition in NFκB may be due to FAC@CurP-SeNPs ability to inhibition IκBα. Overproduction of ROS results in accumulation of oxidative products of DNA, such as DNA strand breaks (DSBs), DNA intra-strand adducts and DNA–protein crosslinks[56, 57]. In response to DSBs, ATM andATR phosphorylate various downstream substrates, such as CHK1 and CHK2, H2AX and p53, to trigger cell apoptosis. p53 is a tumor suppressor gene that plays a critical role in the cell apoptosis by regulating the transcription of a wide variety of genes involved in cell apoptosis, such as p21, Bax, Fas, PUMA and Bid[58, 59]. As shown in Fig. 6C, treatment of FAC@CurP-SeNPs resulted in enhancements of phosphorylated ATM, phosphorylated Brca1, phosphorylated p53, and Ser 139-Histone H2A.X, a maker of DNA damage, was also up-regulated in treated cells. These results demonstrate the involvement of ROS-activated p53 signaling pathway after treatment with FAC@CurP-SeNPs. And FAC@CurP-SeNPs exhibited higher upregulation activity than treated with CurP or FAC-SeNPs alone (Fig. 6B). In this study, we show that, FAC@CurP-SeNPs significantly triggered the phosphorylation of histone at Ser 139 site, indicating that FAC@CurP-SeNPs triggers cancer cell apoptosis through DNA damage-mediated p53 activation.

The main source of ROS inside the cells was the mitochondrial respiratory[60]. Mitochondria act as a point of integration for apoptotic signals originating from both the extrinsic and intrinsic pathways. JC-1 flow cytometric analysis was performed to evaluate the depletion of mitochondrial membrane potential (ΔΨm). As shown in Fig. 7A, depletion of

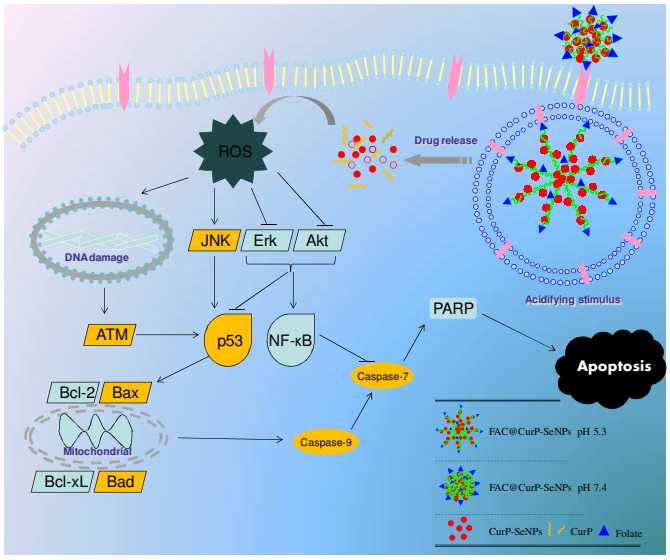

Fig. 8. Proposed signaling pathways of apoptosis induced by FAC@CurP-SeNPs. Acidifying stimulus lead to drug release of FAC@CurP-SeNPs resulted in causing ROS accumulation. FAC@CurP-SeNPs induce DNA damage, AKT and ERK dephosphorylation and result in the activation of p53 pathway and the inhibition of NFκB pathway, which in turn trigger mitochondrial dysfunction to amplify the apoptotic signals.

ΔΨm increased from 8.0% to 89.1% after treatment with FAC@CurP-SeNPs for 24 hours in MCF-7 cells. These results revealed that mitochondria-mediated apoptotic pathway contributes to FAC@CurP-SeNPs-induced apoptosis. Bcl-2 family members have been identified as key regulators of mitochondria permeability. Therefore, we examined the effects of FAC@CurP-SeNPs on the expression levels of pro-survival and pro-apoptotic Bcl-2 family proteins in MCF-7 cells. As shown in Fig. 7B and C, FAC@CurP-SeNPs significantly increased the expression of the proapoptosis protein Bad and Bax in a dose-dependent manner. FAC@CurP-SeNPs exhibited higher upregulation activity than treated with CurP or FAC-SeNPs alone. Taken together, our results indicate that, Acidifying stimulus lead to drug release of FAC@CurP-SeNPs resulted in causing ROS accumulation. FAC@CurP-SeNPs induce DNA damage, AKT and ERK dephosphorylation and result in the activation of p53 pathway and the inhibition of NFκB pathway, which in turn trigger mitochondrial dysfunction to amplify the apoptotic signals (Fig. 8).

4 Conclusions

In conclusion, we present a cancer-targeted drug delivery system that allows the direct fluorescence monitoring of the cellular uptake and localization of theranostic agents in cancer cells, by the combination of robust inorganic SeNPs with the high diversity surface flexibility materials-chitosan and using folate acid as a targeting ligand. This nanosystem exhibits characteristic of shape transformation and pH-controlled drug release that allow the facilitated release of entrapped CurP within acidifying intracellular compartments such as endosomes and lysosomes. Taken together, this study provides a strategy for design and fabrication of cancer-targeted

inorganic capsules, and opens a new path for treatment of cancer with higher efficacy and decreased side effects.

Acknowledgements

This work was supported by National High Technology Research and Development Program of China (863 Program, SS2014AA020538), Science Foundation for Distinguished Young Scholars of Guangdong Province, Natural Science Foundation of China and Guangdong Province, Program for New Century Excellent Talents in University, YangFan Innovative & Entepreneurial Research Team Project, Research Fund for the Doctoral Program of Higher Education of China and China Postdoctoral Science Foundation.

Notes and references

[a] Department of Chemistry, Jinan University, Guangzhou 510632, China. E-mail: tchentf@jnu.edu.cn, tzhwj@jnu.edu.cn

[b] School of Life Science and State Key Laboratory for Agrobiotechnology, The Chinese University of Hong Kong, Hong Kong S.A.R, China. E-mail: yumshingwong@cuhk.edu.hk

† Footnotes should appear here. These might include comments relevant to but not central to the matter under discussion, limited experimental and spectral data, and crystallographic data.

Electronic Supplementary Information (ESI) available: [details of any supplementary information available should be included here]. See DOI: 10.1039/b000000x/

1. V. Wagner, A. Dullaart, A. K. Bock and A. Zweck, *Nat. Biotechnol.*, 2006, **24**, 1211-1217.
2. M. B. Bindu, B. Kusum and B. David, *Int. J. Pharm.*, 2010, **4**, 8-76.
3. J. Ferlay, D. M. Parkin and E. Steliarova-Foucher, *Eur. J. Cancer*, 2008, **46**, 765-781.
4. H. Hu, C. Jiang, T. Schuster, G. X. Li, P. T. Daniel and J. Lu, *Mol.cancer ther.*, 2006, **5**, 1873-1882.
5. D. Peer, J. M. Karp, S. Hong, O. C. FaroKHzad, R. Margalit and R. Langer, *Nat. Nanotechnol.*, 2007, **2**, 751-760.
6. S. Y. Shieh, M. Ikeda, Y. Taya and C. Prives, *Cell*, 1997, **91**, 325-334.
7. A. D. Dinsmore, M. F. Hsu, M. G. Nikolaides, M. Marquez, A. R. Bausch and D. A. Weitz, *Science*, 2002, **298**, 1006-1009.
8. L. J. De Cock, S. De Koker, B. G. De Geest, J. Grooten, C. Vervaet, J. P. Remon, G. B. Sukhorukov and M. N. Antipina, *Angew. Chem. Int. Ed.*, 2010, **49**, 6954-6973.
9. S. Mandal, M. Sathish, G. Saravanan, K. K. R. Datta, Q. Ji, J. P. Hill, H. Abe, I. Honma and K. Ariga, *J. Am. Chem. Soc.*, 2010, **132**, 14415-14417.
10. Y. Li, X. Li, Y.-S. Wong, T. Chen, H. Zhang, C. Liu and W. Zheng, *Biomaterials*, 2011, **32**, 9068-9076.
11. R. Haag and F. Kratz, *Angew. Chem. Int. Ed.*, 2006, **45**, 1198-1215.
12. G. g. F. Schneider and G. Decher, *Nano Lett.*, 2008, **8**, 3598-3604.
13. A. Nori and J. Kopeček, *Adv. Drug Delive. Rev.*, 2005, **57**, 609-636.
14. W. J. Stark, *Angew. Chem. Int. Ed.*, 2011, **50**, 1242-1258.
15. S.-W. Choi, Y. Zhang and Y. Xia, *Angew. Chem. Int. Ed.*, 2010, **49**, 7904-7908.
16. R. Guillet-Nicolas, A. Popat, J.-L. Bridot, G. Monteith, S. Z. Qiao and F. Kleitz, *Angew. Chem. Int. Ed.*, 2013, n/a-n/a.
17. Y. Li, W. Xiao, K. Xiao, L. Berti, J. Luo, H. P. Tseng, G. Fung and K. S. Lam, *Angew. Chem. Int. Ed.*, 2012, **51**, 2864-2869.
18. Y. Qiu and K. Park, *Adv Drug Deliv Rev*, 2001, **53**, 321-339.
19. K. Riehemann, S. W. Schneider, T. A. Luger, B. Godin, M. Ferrari and H. Fuchs, *Angew. Chem. Int. Ed.*, 2009, **48**, 872-897.
20. M. Vallet-Regí, F. Balas and D. Arcos, *Angew. Chem. Int. Ed.*, 2007, **46**, 7548-7558.
21. Y. Zhu, W. Meng, H. Gao and N. Hanagata, *J. Phys. Chem. C*, 2011, **115**, 13630-13636.
22. J. L. Wu, F. Qin, F. Y. F. Chan, G. Cheng, H. Li, Z. Lu and R. Chen, *Mater. Lett.*, 2010, **64**, 287-290.
23. Y. Wang, Y. Yan, J. Cui, L. Hosta-Rigau, J. K. Heath, E. C. Nice and F. Caruso, *Adv. Mater.*, 2010, **22**, 4293-4297.
24. Z. Zhou, Y. Shen, J. Tang, M. Fan, E. A. Van Kirk, W. J. Murdoch and M. Radosz, *Adv. Funct. Mater.*, 2009, **19**, 3580-3589.
25. C. Hu, G. Song, B. Zhang, Z. C. Liu, R. Chen, H. Zhang and T. H. Hu, *J. Cell. Mol. Med.*, 2012, **16**, 96-106.
26. Q. Ji, C. Guo, X. Yu, C. J. Ochs, J. P. Hill, F. Caruso, H. Nakazawa and K. Ariga, *Small*, 2012, **8**, 2345-2349.
27. J.-S. Yu, S. B. Yoon, Y. J. Lee and K. B. Yoon, *J. Phy. Chem. B*, 2005, **109**, 7040-7045.
28. M. Kim, K. Sohn, H. B. Na and T. Hyeon, *Nano Lett.*, 2002, **2**, 1383-1387.
29. F. Yang, Q. M. Tang, X. Y. Zhong, Y. Bai, T. F. Chen, Y. B. Zhang, Y. H. Li and W. J. Zheng, *Int. J. Nanomed.*, 2012, **7**, 835-844.
30. L. Kong, Q. Yuan, H. Zhu, Y. Li, Q. Guo, Q. Wang, X. Bi and X. Gao, *Biomaterials*, 2011, **32**, 6515-6522.
31. C. M. Weekley, J. B. Aitken, I. F. Musgrave and H. H. Harris, *Biochemistry*, 2012, **51**, 736-738.
32. J. Zhang, X. Wang and T. Xu, *Toxicol. Sci.*, 2008, **101**, 22-31.
33. Y. Min, C.-Q. Mao, S. Chen, G. Ma, J. Wang and Y. Liu, *Angew. Chem. Int. Ed.*, 2012, **51**, 6742-6747.
34. Y. Huang, L. He, W. Liu, C. Fan, W. Zheng, Y. S. Wong and T. Chen, *Biomaterials*, 2013, **34**, 7106-7116.
35. H. Tang, C. J. Murphy, B. Zhang, Y. Shen, E. A. Van Kirk, W. J. Murdoch and M. Radosz, *Biomaterials*, 2010, **31**, 7139-7149.
36. S. Reuter, S. Eifes, M. Dicato, B. B. Aggarwal and M. Diederich, *Biochem. Pharmacol.*, 2008, **76**, 1340-1351.
37. C. Y. Gong, S. Y. Deng, Q. J. Wu, M. L. Xiang, X. W. Wei, L. Li, X. Gao, B. L. Wang, L. Sun, Y. S. Chen, Y. C. Li, L. Liu, Z. Y. Qian and Y. Q. Wei, *Biomaterials*, 2013, **34**, 1413-1432.
38. S. Manju and K. Sreenivasan, *Langmuir*, 2011, **27**, 14489-14496.
39. S.-J. Yang, F.-H. Lin, K.-C. Tsai, M.-F. Wei, H.-M. Tsai, J.-M. Wong and M.-J. Shieh, *Bioconjugate. Chem.*, 2010, **21**, 679-689.
40. B. Yu, T. F. Chen, F. Yang, W. Liu, Y. H. Li and W. J. Zheng, *Chem. Lett.*, 2011, **40**, 242-243.
41. S. Manju and K. Sreenivasan, *J.Pharm. Sci.*, 2011, **100**, 504-511.
42. W. Liu, X. Li, Y.-S. Wong, W. Zheng, Y. Zhang, W. Cao and T. Chen, *ACS Nano*, 2012, **6**, 6578-6591.
43. M. Hao, A. M. Lowy, M. Kapoor, A. Deffie, G. Liu and G. Lozano, *J. biol. chem.*, 1996, **271**, 29380-29385.
44. S. Zheng, X. Li, Y. Zhang, Q. Xie, Y. S. Wong, W. Zheng and T. Chen, *Int. J. Nanomed.*, 2012, **7**, 3939-3949.
45. B. Yu, Y. Zhang, W. Zheng, C. Fan and T. Chen, *Inorg Chem*, 2012, **51**, 8956-8963.

46. H. Tang, C. J. Murphy, B. Zhang, Y. Shen, E. A. Van Kirk, W. J. Murdoch and M. Radosz, *Biomaterials*, 2010, **31**, 7139-7149.
47. H. Wu, H. Zhuzhu, X. Li, Z. Li, W. Zheng, T. Chen, B. Yu and K. H. Wong, *J. Agric. Food. Chem.*, 2013.
48. I. M. Fang, C.-H. Yang, C.-M. Yang and M.-S. Chen, *PLoS One*, 2013, **8**, e77323.
49. J. Ghosh, J. Das, P. Manna and P. C. Sil, *Biomaterials*, 2011, **32**, 4857-4866.
50. S. Krifka, C. Petzel, C. Bolay, K. A. Hiller, G. Spagnuolo, G. Schmalz and H. Schweikl, *Biomaterials*, 2011, **32**, 1787-1795.
51. M. K. Guenther, U. Graab and S. Fulda, *Cancer Lett*, 2013, **337**, 200-209.
52. F. Chiacchiera, V. Grossi, M. Cappellari, A. Peserico, M. Simonatto, A. Germani, S. Russo, M. P. Moyer, N. Resta, S. Murzilli and C. Simone, *Cancer Lett*, 2012, **324**, 98-108.
53. R. Al-Halabi, M. Bou Chedid, R. Abou Merhi, H. El-Hajj, H. Zahr, R. Schneider-Stock, A. Bazarbachi and H. Gali-Muhtasib, *Cancer Biol Ther*, 2011, **12**, 59-68.
54. N. Bakkar, K. Ladner, B. D. Canan, S. Liyanarachchi, N. C. Bal, M. Pant, M. Periasamy, Q. Li, P. M. Janssen and D. C. Guttridge, *J Cell Biol*, 2012, **196**, 497-511.
55. C. J. Wright, F. Agboke, M. Muthu, K. A. Michaelis, M. A. Mundy, P. La, G. Yang and P. A. Dennery, *J. Biol. Chem.*, 2012, **287**, 6230-6239.
56. J. Su, H. Lai, J. Chen, L. Li, Y. S. Wong, T. Chen and X. Li, *PLoS One*, 2013, **8**, e63502.
57. A. Kotsinas, V. Aggarwal, E. J. Tan, B. Levy and V. G. Gorgoulis, *Cancer Lett.*, 2012, **327**, 97-102.
58. Angelina V. Vaseva, Natalie D. Marchenko, K. Ji, Stella E. Tsirka, S. Holzmann and Ute M. Moll, *Cell*, 2012, **149**, 1536-1548.
59. J. P. Kruse and W. Gu, *Cell*, 2009, **137**, 609-622.
60. C. Liu, Z. Liu, M. Li, X. Li, Y. S. Wong, S. M. Ngai, W. Zheng, Y. Zhang and T. Chen, *PLoS One*, 2013, **8**, 14.